metals

MDPI

Article

Comparison of Different Manufacturing Processes of AISI 4140 Steel with Regard to Surface Modification and Its Influencing Depth

Florian Borchers [1], Brigitte Clausen [2,*], Sandro Eckert [3], Lisa Ehle [4], Jeremy Epp [1], Simon Harst [5], Matthias Hettig [2], Andreas Klink [5], Ewald Kohls [1], Heiner Meyer [1], Markus Meurer [5], Bob Rommes [5], Sebastian Schneider [5] and Rebecca Strunk [1]

1 Leibniz-Institute for Materials Engineering-IWT Bremen, Badgasteiner Str. 3, 28359 Bremen, Germany; borchers@iwt-bremen.de (F.B.); epp@iwt-bremen.de (J.E.); kohls@iwt-bremen.de (E.K.); hmeyer@iwt-bremen.de (H.M.); strunk@iwt-bremen.de (R.S.)

2 RG 11: Materials Engineering/Metals, Faculty of Production Engineering, University of Bremen, Badgasteiner Str. 1, 28359 Bremen, Germany; hettig@iwt-bremen.de

3 BIAS—Bremer Institut für angewandte Strahltechnik GmbH, Klagenfurter Straße 5, 28359 Bremen, Germany; mail@seckert.de

4 Central Facility for Electron Microscopy (GFE), RWTH Aachen University, RWTH-Gebäude-Nr. 2356, Ahornstraße 55, 52074 Aachen, Germany; ehle@gfe.rwth-aachen.de

5 Laboratory for Machine Tools and Production Engineering (WZL) of RWTH Aachen University, Campus-Boulevard 30, 52074 Aachen, Germany; simon.harst@zv.fraunhofer.de (S.H.); a.klink@wzl.rwth-aachen.de (A.K.); m.meurer@wzl.rwth-aachen.de (M.M.); b.rommes@wzl.rwth-aachen.de (B.R.); s.schneider@wzl.rwth-aachen.de (S.S.)

* Correspondence: clausen@iwt-bremen.de; Tel.: +49-421-218-51355

Received: 19 May 2020; Accepted: 29 June 2020; Published: 5 July 2020

Abstract: The surface and subsurface conditions of components are significant for their functional properties. Every manufacturing process step changes the surface condition due to its mechanical, chemical and/or thermal impact. The depth of the affected zone varies for different machining operations, and is predetermined by the process parameters and characteristics. Furthermore, the initial state has a decisive influence on the interactions that lead to the final surface conditions. The aim of the investigation presented here is to compare the influence of the load characteristics over the depth applied to manufactured components by several different machining operations and to determine the causing mechanisms. In order to ensure better comparability between the surface modifications caused by different machining operations, the same material was used (AISI 4140; German steel grade 42CrMo4 acc. to DIN EN 10083-3) and annealed to a ferritic-pearlitic microstructure. Based on interdisciplinary cooperation within the collaborative research center CRC/Transregio 136 "Process Signatures", seven different manufacturing processes, i.e., grinding, turning, deep rolling, laser processing, inductive heat treatment, electrical discharge machining (EDM) and electrochemical machining (ECM), were used, and the resulting surface zones were investigated by highly specialized analysis techniques. This work presents the results of X-ray measurements, hardness measurements and electron microscopic investigations. As a result, the characteristics and depths of the material modifications, as well as their underlying mechanisms and causes, were studied. Mechanisms occurring within 42CrMo4 steel due to thermal, mechanical, chemical or mixed impacts were identified as phase transformation, solidification and strengthening due to dislocation generation and accumulation, continuum dynamic recrystallization and dynamic recovery, as well as chemical reactions.

Keywords: surface integrity; influencing depth; XRD; SEM; TEM; EBSD; hardness

1. Introduction

1.1. Surface Integrity

The surface properties of machined components are influenced by machining operations that determine their geometry. Due to material removal and the applied thermal, mechanical and chemical loads, the local mechanical properties, the residual stress state, and the microstructure are changed [1]. This change in the surface condition is known to influence the component's performance, e.g., fatigue strength [2,3]. The transregional collaborative research center CRC/Transregio 136 "Process Signatures" aims to describe processes by assessing correlations between internal loads, like temperature and strain fields, and the resulting surface modifications, like grain size, hardness or residual stresses. These correlations will allow inverse problems to be solved and will give rise to parameter-independent dimensioning of machining processes [4].

The topic of surface integrity has been addressed by many authors, since its importance has become evident. Surface integrity and the importance of microstructures for electrochemical machining (ECM) processes were recently investigated, for example in [5,6]. The influence of roughness on part performance for electrical discharge machining (EDM) is, for example, described in [7] for plastic injection molding. Considering deep rolling, the influence on surface integrity has been investigated by many authors regarding different aspects. The authors of [8] and [9] describe the influence of deep rolling on hardness and residual stresses on the surface and subsurface layer for hardened steel. The authors of [10,11] investigated deep rolling as a technology for efficient lightweight design, focusing on the vibration resistance of the final part, also regarding the surface and subsurface influence of the hardness, roughness and residual stresses. A good overview regarding general surface integrity aspects for hybrid processes is given in [12]. However, the results from individual investigations cannot be compared directly.

In the CRC, surface conditions after machining are investigated with X-ray diffraction, hardness measurements and light and electron microscopic methods. In the beginning, a large number of different machined surface conditions were analyzed by the subprojects, providing the analysis techniques. For example, Klocke et al. undertook an intense investigation of white layers, which occurred after applying an EDM process [13]. Ehle et al. published an investigation of surface modifications, determined using an electron microscope, due to deep rolling [14]. Heinzel et al. investigated surface modifications which occur due to precision grinding [15]. A comparison of the different results was, despite the use of a common material with uniform heat treatment, a complex undertaking due to different sample geometries and premachining conditions. In particular, it was difficult for the subprojects to guess in advance which magnification or analysis depth would be suitable for which machining process. The working group "Material Modifications and Analysis of Mechanisms" was used as a platform to bring together the interests of the analysis and machining projects. Two sample geometries which were machinable by the majority of the projects were developed. Heat treatment and premachining were carried out identically for these samples. First, 100 µm of the surface was gently removed electrochemically after the last premachining step, in order to remove any thermomechanical influences and minimize chemical influences. The samples were machined in a defined way by the machining subprojects, divided into four pieces and distributed to the various project members. The results of the analyses were presented and discussed in a working group.

In this paper, the applied machining and analysis techniques are described, and selected results are presented. The uniform experimental design provides a rational basis to compare the material modifications of machining processes with mechanical, thermal and chemical impacts.

1.2. Process Fundamentals on Machining Operations

In this paper, the influence of machining operations on the surface integrity of the material is compared. The operations were selected due to their different impacts on the surface (Figure 1). While deep rolling and grind strengthening exert a primarily mechanical influence on the surface,

grinding and hard turning exert an additional thermal influence. A pure thermal influence was provided using a pulsed (µs) laser process or induction hardening process. EDM has a main thermal influence, but the surface can additionally, under certain boundary conditions (e.g., rough machining with reduced flushing), be slightly influenced chemically. Since this also happened in this study, the process is not positioned in the triangle corner, but moved slightly in the chemical direction. The impact of ECM on the surface is purely chemical. The processes are described in detail below.

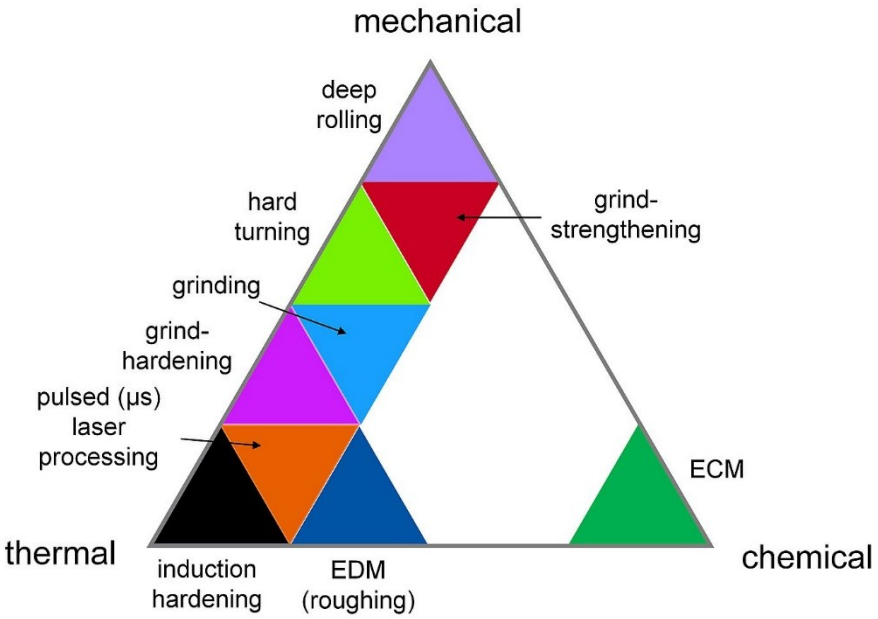

Figure 1. The impact of machining operations on the machined surface (the same color code is used in the comparison of the analysis results).

1.2.1. Deep Rolling

Deep rolling induces a purely mechanical load on the workpiece and is a nonmaterial-removing process. During deep rolling, a deep rolling tool is pressed against the surface of the workpiece with a defined force F_r. This force can be generated mechanically or hydrostatically by applying hydraulic pressure. Hardened rollers or ceramic spheres with varying diameters are used as tools. The tool is routed over the workpiece surface with a deep rolling velocity v_{dr} and a feed rate f_{dr} which is orthogonal to v_{dr}. The tools can be used on conventional CNC lathes or milling machines in combination with conventional tools. The process is used to achieve a work hardening of the surface with a decrease in roughness and an increase in compressive residual stresses.

1.2.2. Grinding

Grinding is a thermo-mechanical process with geometrically undefined cutting edges. High surface quality, in combination with a high degree of accuracy, are good reasons to use grinding processes. When grinding is applied at the end of a production chain, it plays a big part in defining the surface state and quality of the finished part. Today, grinding is not only used as a finishing process, but also as a highly efficient process with high material removal rates. Also, grinding can be applied for processing materials that are hard to cut [16,17].

Due to its versatile input parameters (e.g., grinding wheel specification and the choice of cooling lubricant), as well as process parameters, its impact can range from predominantly thermal (grind hardening) to predominantly mechanical (grind strengthening).

1.2.3. Grind Strengthening

Grind strengthening is a grinding process with focus on a dominating mechanical impact, whereby the mechanical load on the workpiece surface and the mechanically induced material modifications are enhanced. For this purpose, the size effect of the specific grinding energy is an important aspect [18]. As a result, the chip thickness is reduced, and proportions of the working mechanisms of the material removal are shifted to mechanical deformation mechanisms and an increase of elastic and plastic deformation, e.g., plowing and grooving. The mechanical impact, combined with material removal, can result in surface properties such as compressive residual stress depth profiles, which can have positive effects on the surface integrity and, e.g., the wear-resistance of steel workpieces [18]. The mechanical impact can be affected by the process parameters, e.g., low cutting speed v_c or the layout of the grinding wheel [15].

1.2.4. Grind Hardening

High thermal material loads can lead to tempered zones and brittle hardening zones, also known as "grinding burn". Excessive thermal impact during grinding can lead to a decrease in the fatigue strength of the material, which is the reason why it is usually avoided [4]. An exception, in which the high heat input during grinding is desirable, is the so-called grind hardening process of heat treatable steels. The main advantage of these processes is the combination of short heat treatment and material removal, resulting in a shortened process chain. In grind hardening processes, diffusion and phase transformation processes take place if the surface layer material is heated above the material's austenitization temperature during grinding. After the heating phase, the high temperature gradients in the surface layer lead to quenching. As a result, very fine-grained martensitic structures in the form of parallel needles within former austenite grains are generated. The content of carbon and alloying elements, as well as the pretreatments, are the main factors influencing the hardening mechanism [19].

1.2.5. Hard Turning

Hard turning, as a variant of cutting processes, has a heavy thermo-mechanical impact upon the workpiece. Residual austenite formation, work hardening, white layer formation and residual stress state changes may result. While the prediction of the exact surface integrity features is of increasing importance, it remains dependent on complex interactions among numerous process conditions. For this reason, Figure 2 shows a qualitative comparison of the influence of individual process variables on the residual stress state during hard turning [20,21].

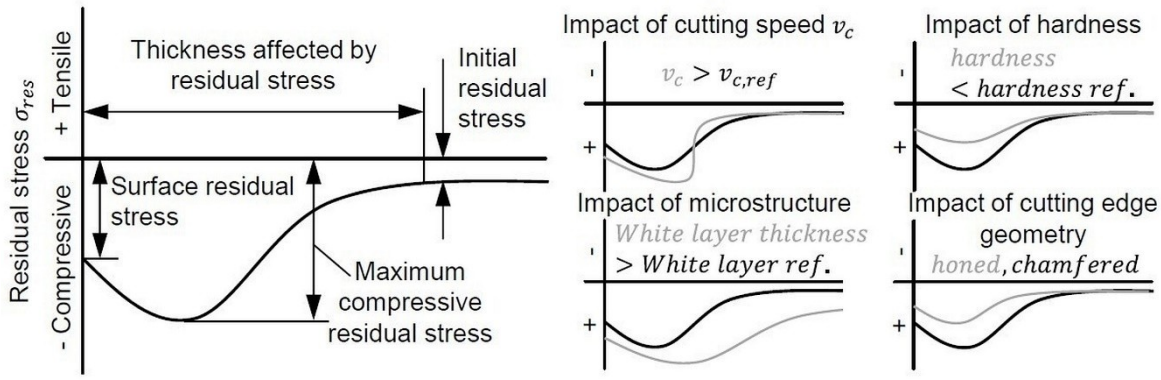

Figure 2. Stresses induced by hard turning and the qualitative impacts of the tool, process and initial material parameters [20,21].

1.2.6. Induction Hardening

Inductive heat treatment has a purely thermal impact on the component surface. It is based on the physical principles of inducing eddy currents into the component, and can be applied to all

electrically conductive materials [22,23]. Typical applications are surface layer hardening, forging or tempering. Induction heating shortens the time for heat treatment because of the rapid heating of the workpiece [22,24,25].

The main components of an induction facility are the power supply, the inductor, a load-matching system and the workpiece itself. Inductors exist in many different shapes and sizes, each designed for the application at hand [26]. In this investigation, an inner field inductor was used. The workpiece was moved through the inductor coil during the heating process. For good operating conditions, an even distance between the workpiece and the induction coil is needed, which is referred to as the coupling gap. The coupling gap should be minimal for the best heating results [26].

1.2.7. Pulsed (µs) Laser Processing

Microsecond pulsed laser processing is a noncontact, wear-free, thermal material processing method. It offers highly flexible and direct manipulation of the material. A great variety of materials like pure metals, alloys and high-strength materials, but also ceramics, semiconductors, plastics and multilayer materials can be processed [27]. Depending on the application and laser power, the process can be used for melting (~10^8 W/cm^2) and sublimation drilling [28], cutting [29] or material removal [30] applications. Material removal is caused by evaporation or ejection of the molten material. Melt ejection can be achieved either by applying an external gas flow or by the recoil pressure of the emerging evaporation of the material [31]. As a result, the melt flows and gets ejected radially from the laser irradiated center. The high material removal velocity (several mm/s) go along with residual debris, melt deposits and a decrease in precision. To minimize melt deposits and the recast zone, the surface can be additionally processed by means of laser sublimation material removal. Nevertheless, the rim zone is affected by the laser induced heat and phase transformations, as well as possible recast layers [32]. These depend significantly on the process parameters and melt ejection efficiency. By scanning the laser radiation along the surface, the selective removal of a 2D micro- or macroscopic area is possible.

1.2.8. Electrical Discharge Machining

Electrical discharge machining (EDM) is a thermal main active principle processing technology. It is possible to machine all electrically conductive materials, regardless of their mechanical properties [33], which is an advantage for the machining of hard and brittle materials [34] or filigree structures [35]. The removal principal is based on electrical discharges between two electrically isolated electrodes (Figure 3). For insulation, the process takes place in dielectric fluids. Hydrocarbon-based dielectrics are most common, but deionized water or gaseous media are also used. An open circuit voltage is applied to the electrodes, and consequently, an electrical field occurs between them. In the next step, the distance between the electrodes is reduced until the electrical field exceeds the dielectric strength of the gap and discharge occurs. Thereby, a plasma channel is formed, allowing the current to flow. The heat of the plasma melts and evaporates, and hence, removes material from the workpiece, as well as a small amount of the tool electrode. The discharge duration, meaning the time of the current flow, can typically be adjusted from <1 µs to 1000 µs. This procedure is repeated at high frequencies to achieve acceptable material removal rates. In this way, the tool geometry is formed in the workpiece material. As material removal at the anodic electrode is different to that at the cathodic electrode, this process is economically viable.

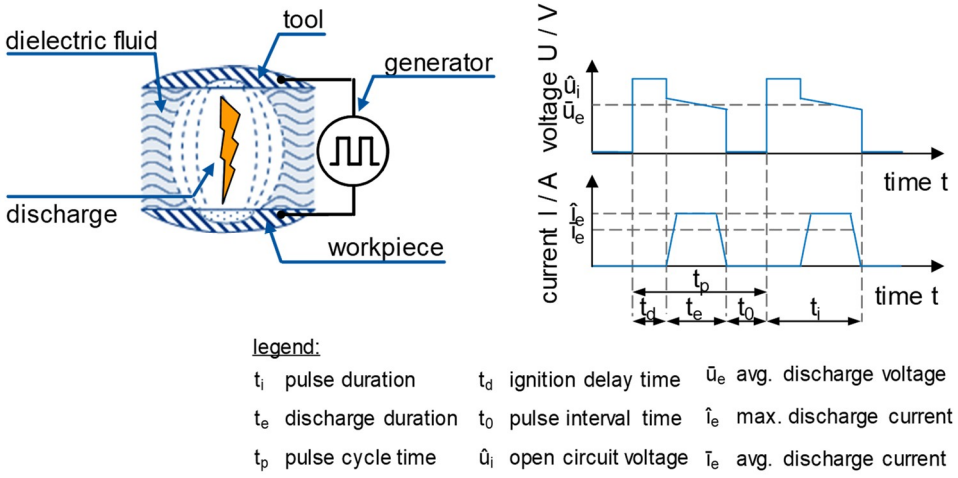

Figure 3. Principal of electrical discharge machining and relevant characteristic values [36].

Due to the thermal removal mechanism, the rim zone is highly affected by the process. The temperature and its spatial and temporal gradients result in the most significant material loads [37]. These thermal loads result in superimposed mechanical stresses due to thermal expansion [38]. Measurement of the temperature field during this process is very challenging, due to the short cycle times and small discharge spots. The only established method to get information about the inner material temperature is by using the heat transfer equation [39,40] or the solution of the inverse problem, by using the material modifications and the underlying mechanisms to calculate temperature gradients [41].

According to the idea of process signatures, the described material loads lead to material modifications. The main modifications which occur are phase transformations due to temperatures above the austenitization temperature (heat affected zone = HAZ), and resolidified melt (recast layer = RL) due to temperatures above the melting point [42].

1.2.9. Electrochemical Machining

The underlying principle of material removal during electrochemical machining (ECM) is electrolysis, which is defined as the chemical processes caused by an electric current passing through an electrolyte [36]. During ECM, the electrolyte flows through a small gap between two metallic electrodes. One of these electrodes corresponds to the workpiece, while the other is the machining tool. To create the required electric current, a certain voltage is applied to the electrodes, causing material to be removed from the positively charged workpiece (anode). This process offers high material removal rates, even for high-strength and heat resistant materials, which is a huge benefit compared to more traditional processes such as milling. Moreover, no mechanical or thermal stresses are introduced into the workpiece, as only moderate mechanical forces and temperatures occur. Furthermore, since material removal takes place on an atomic scale, excellent surface qualities can be achieved, without the need for postprocessing. This feature is visually represented by the shiny surface of the finished workpiece.

2. Materials and Methods

2.1. Uniform Starting Position

First, a simple geometry which was suitable for several different machining operations provided within the CRC was defined. The machining operations applied on rotating components used a cylinder with a diameter of 58 mm (57.8 mm after the electrochemical removal of the surface layer). Subprojects that could apply their machining operations only on flat surfaces, used cuboids. The steel for all samples was the standard material which has been used in investigations within this CRC since 2015 (Table 1). The samples were manufactured and heat treated at the Leibniz-Institute for Materials

Engineering - IWT Bremen with the same parameters to a ferritic-pearlitic microstructure (211 HV 1). To provide a suitable initial state, the heat treated surface was removed gently by electro polishing in an electrolyte with 45 weight-% phosphoric acid and 35 weight-% sulfuric acid. The etching depth was set to 100 µm to remove any material influenced by the heat treatment, carbon diffusion or premachining processes. This led to an initial material state, as measured by X-ray diffraction, with a FWHM of 0.56–0.04° and less than 40 MPa residual stresses.

Table 1. Chemical composition of the steel used in all investigations presented in this work.

Notation Unit	C %	Cr %	Mn %	P %	S %	Si %	Mo %	Ni %	Al %	Cu %
AISI 4140 42 CrMo 4	0.448	1.09	0.735	0.012	0.002	0.264	0.244	0.200	0.018	0.065

The samples were distributed to the projects and the machining operations, described in the following chapter, were applied. After machining, the samples were cut into four pieces and distributed to the analysis subprojects.

2.2. Machining Operations

To give an overview on the impacts of different machining operations, only one set of standard parameters for machining the given material was chosen at a time. The following chapters provide the machining conditions and parameters in detail.

2.2.1. Deep Rolling

Deep rolling was conducted on a CNC turning machine at the Leibniz-Institute for Materials Engineering-IWT Bremen. The diameter of the sample was d_w = 57.8 mm, and the length l = 100 mm. To conduct the process, a hydrostatical deep rolling tool was used. Hydrostatic deep rolling is a force-controlled process. The height adapting tool provides a constant hydraulic pressure which transmits the necessary force. The applied force remains constant, even if slight height differences occur during the process. A single-pass deep rolling operation was conducted on the surface using the parameters given in Table 2. The parameters were chosen with the aim of introducing high residual compression stresses while creating a smooth surface.

Table 2. Parameters for deep rolling operation.

Parameter	Ball Diameter	Deep Rolling Pressure	Deep Rolling Force	Feed	Deep Rolling Velocity
Abr. [unit]	d_k [mm]	p_{dr} [bar]	F_{dr} [N]	f_{dr} [mm/U]	v_{dr} [mm/min]
value	6	400	1130	0.55	100

2.2.2. Grind Strengthening

To investigate the mechanical impact of grinding, a cylindrical grinding process was designed and adjusted to increase the mechanical load and reduce the thermal load. Grind strengthening was conducted on a high precision cylindrical grinding machine (Studer S41) at the Leibniz-Institute for Materials Engineering—IWT Bremen. The diameter of the workpieces before grinding was d_w = 57.8 mm, and the width was b_w = 12.0 mm.

The grinding wheel was a vitrified bond corundum wheel with a medium grain size. The specification of the grinding wheel was A60K5AV. To avoid further impact on the specimens, no preliminary grinding was applied before the experiment. Hence, the workpieces had to be adjusted precisely in the machine to achieve direct uniform material contact. The process was performed in three stages. The grinding parameters are provided in Table 3. In the presented experiments, notably,

the cutting speed v_c and the radial feed speed were selected in a low range so that the grinding process would promote the desired low thermal load and material modification behavior.

Table 3. Parameters for grind strengthening operation.

Parameter	Cutting Speed	Radial Feed	Depth of Cut	Max. Normal Force	Max. Tangential Force
Abr. [unit]	v_c [m/s]	v_{fr} [mm/min]	a_e [mm]	F_n [N]	F_t [N]
value	1	0.3/0.1/0.024	0.1/0.02/0.01	134	99

Grinding oil was used as a coolant and the flow rate was adjusted to Q_{MWF} = 60 L/min. The grinding wheel, dressing setup and dressing parameters were kept constant throughout the experiments. As material loads process forces F_n and F_t, were obtained during the grinding experiments for all process stages. The measurements were taken by a machine-integrated force measurement system. The maximum values of the measured forces over the complete process, which occurred at the first process stage at a radial feed of v_{fr} = 0.3 mm/min, are given in Table 3.

2.2.3. Grind Hardening

The grind hardening test was performed on the surface grinding machine Blohm Profimat 412 HSG at the Leibniz Institute for Materials Engineering—IWT Bremen using a corundum grinding wheel type A80HH9V with a width of 30 mm and a diameter of 392 mm. The grind-hardened workpiece was a cuboid with a length of 150 mm, a width of 30 mm and a depth of 18 mm. The test was done in up-grinding mode with a wheel speed of vs. = 35 m/s. White mineral oil was supplied at a flow rate of Q_{MWF} = 45 L/min. The process parameters (Table 4) were chosen due to the fact that the temperatures generated during grinding were above the austenitization temperature, leading to phase transformations.

Table 4. Parameters for grind hardening operation.

Parameter	Specific Material Removal Rate	Tangential Feed	Depth of Cut	Geometrical Contact Length	Contact Time
Abr. [unit]	Q'_w [mm^3/(mm·s)]	v_{ft} [mm/min]	a_e [mm]	l_g [mm]	t_c [s]
value	8.2	0.7	0.7	16.57	1.42

2.2.4. Hard Turning

The samples were machined with the standard process parameters on a CTX 520 linear CNC lathe (Gildemeister, Bielefeld, Germany). Cemented carbide tools were used with a CVD MT-(Ti(Cn,N) + TiN + Al_2O_3) coating. The cutting parameters were set to a cutting speed v_c = 100 m/min and an uncut chip thickness of h = 0.1 mm. The parameters were chosen to obtain an optimal balance between a smooth surface and a high material removal rate.

2.2.5. Induction Hardening

The inductive heat treatment was carried out in an induction heat treatment plant with a multifrequency concept by EFD Induction at the Leibniz Institute for Materials Engineering—IWT Bremen. The plant works in a middle frequency range, i.e., from 10 to 15 kHz, and in a high frequency range, i.e., between 100 and 200 kHz. The power in total was 300 kW. The parameters applied to the samples are summarized in Table 5. The parameter set was determined in pretrials to guarantee the homogeneous austenitic transformation of the surface area.

Table 5. Parameters for inductive heat treatment operation.

Parameter	Length of Inductor	Feed	Maximal Current	Current at Inductor	Frequency
Abr. [unit]	l [mm]	v_{ft} [mm/s]	I_{max} [A]	I_i [A]	f [kHz]
value	18	900	478	456	10.8

2.2.6. Pulsed (µs) Laser Processing

The experimental setup at the Bremer Institut für angewandte Strahltechnik (BIAS) consisted of a fiber laser (JK400FL, GSI Lumonics, Warwickshire, UK) with a wavelength of 1070 nm and a mean power of 400 W. The laser radiation was guided through optical components (S6EXZ5310/328, Sill Optics GmbH, Wendelstein, Germany) into a scan head (Superscan III-15, Raylase, Wessling, Germany) and focused with a telecentric F-Theta optic (S4LFT3162, Sill Optics GmbH, Wendelstein, Germany), as shown in Figure 4. The laser spot diameter, d_f = 34 µm, was guided onto the surface of the rotational symmetrical sample in a zigzag scan trajectory with a line spacing of b = 9 µm in the y direction, a repetition rate of 1 kHz and a scan velocity of v_L = 9 mm/s. These parameters ensured a pulse overlap of 66% in both the x and y directions. The applied laser power and pulse duration are summarized in Table 6. The laser intensity, $1.3 \cdot 10^7$ W/cm^2, was high enough to cause laser-plasma interactions. The material removal took place by melt ejection and material evaporation. The chosen parameters are typically used for precision drilling and cutting applications.

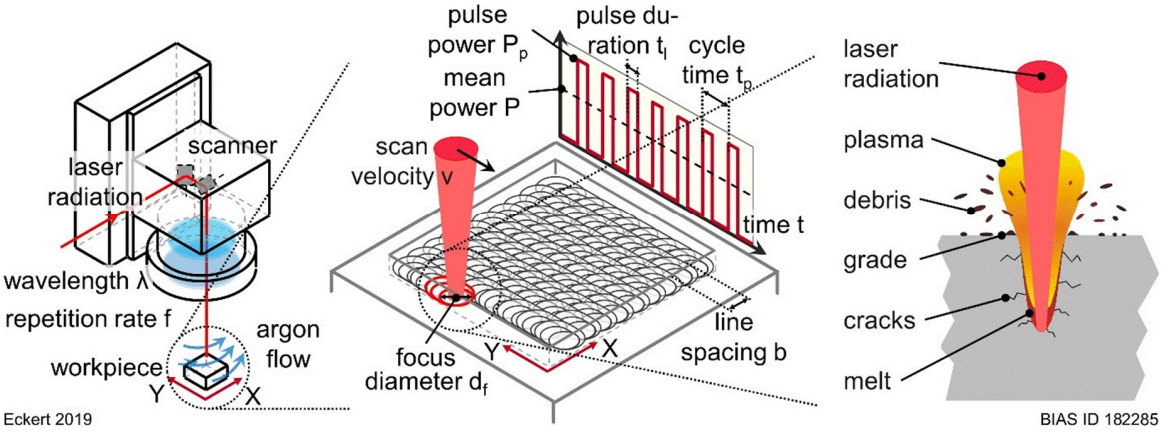

Figure 4. Schematic illustration of the experimental setup, machining setup and parameter and laser-material interaction of pulsed (µs) laser processing.

Table 6. Parameters for pulsed (µs) laser processing operation.

Parameter	Pulse Power	Intensity	Pulse Duration	Cycle Time	Focus Diameter	Scan Velocity	Line Spacing
Abr. [unit]	P_p [W]	I_p [W/cm^2]	t_l [µs]	t_p [µs]	d_f [µm]	v_L [mm/s]	b [µm]
value	120	$1.3 \cdot 10^7$	210	1000	34	9	9

2.2.7. EDM

For the comparison of different manufacturing processes, and hence, different sets of material loads, typical EDM manufacturing parameters were used at the Laboratory for Machine Tools and Production Engineering (WZL) of RWTH Aachen University. The experiments were done on a commercial sinking-EDM machine, the FORM 2000 VHP (GF machining solutions GmbH, Schorndorf, Germany). As dielectric fluid, the hydrocarbon-based dielectric Ionoplus IME-MH, manufactured by Oelheld, was used. The tool was a cuboid made of graphite (grade R8710 by SGL Carbon, Wiesbaden,

Germany). The frontal working area was 15 mm × 15 mm. Adapted to this area, smooth roughing parameters were chosen for the machining (Table 7). The depth of the final cavity was about z = 1 mm.

Table 7. Parameters for EDM operation.

Parameter	Open Circuit Voltage	Discharge Current	Discharge Duration	Pulse Interval Time
Abr. [unit]	$\hat{u}_i$ [V]	I_e [A]	t_e [µs]	t_0 [µs]
value	100	14	20	13.9

2.2.8. ECM

The experimental ECM trials were conducted at the Laboratory for Machine Tools and Production Engineering (WZL) of RWTH Aachen University on an smart PTS 1500 machine tool (EMAG, Gaildorf, Germany) using a working voltage of 19 V. The feed-rate of the tool (cathode) was set to 1 mm/min, resulting in a stationary machining gap throughout the entire sinking process. The electrolyte, a water-based solution of 21 wt.% NaNO3, was pumped between the electrodes at an inlet pressure of 10 bar, which provided an adequate flushing for the removed material and the produced process gas. These parameters are typical for the machining of steel [36].

2.3. Analysing Techniques

To gain information about the characteristics and the depth of the material modifications, the following analysis techniques were used. Martens hardness measurements were used to determine the hardness changes as a function of depth caused by the processes. In contrast to conventional hardness measurements, Martens hardness involves very small forces which are suitable for analyzing small depths.

Electron microscopy with its manifold analysis possibilities provides information concerning microstructural changes and changes on the nano scale.

Based on the measurements of the crystallite structure and changes in the lattice parameters, nondestructive X-ray diffraction analysis could be applied to determine the residual stress state of the processed surface. This is a standard technique in industry for stress validation in highly loaded parts. Additionally, in-depth analysis reveals the constituting crystalline phases and the specific material modifications compared to the initial material state, e.g., changes in crystallite size, texture and dislocation density.

2.3.1. Hardness Measurement

The universal microhardness (UMH) was measured at the Leibniz-Institute for Materials Engineering—IWT Bremen in a cross section of the samples with a Vickers indenter using a Fischerscope H100C (Helmut Fischer GmbH, Sindelfingen, Germany). The testing force was set to 10 mN for 10 s. The Martens hardness was calculated based upon the force depth course, considering the elastic and plastic deformation beneath the indenter, which qualifies it to provide information about the hardness with very small indentations. In order to to place the indentations as close as possible to the surface of the cross sections, three depth profiles were measured running obliquely into the depth of the material. The indentations nearest to the surface did not conform to the standard, and could therefore only be used as indicators of the achieved modification of the material. In the case of the deep rolled samples, the depth profiles were perpendicular to the surface, since deep rolling has a very high depth effect.

2.3.2. Scanning Electron Microscopy (SEM), Energy-Dispersive X-ray Spectroscopy (EDS) and Electron Backscatter Diffraction (EBSD) Measurements

Since light microscopy investigations showed no pronounced difference between the machined samples, overviews of the machined surfaces were obtained on etched cross sections using a scanning

electron microscope. Specimens were embedded in resin, ground, polished and etched with 3% nitric acid (HNO_3) in alcohol. Since the resin is nonconductive, the samples were sputtered with gold after etching. The overviews were taken with a Vega II XLH electron scanning microscope (Tescan GmbH, Dortmund, Germany) at the Leibniz-Institute for Materials Engineering—IWT Bremen.

For further electron microscopy investigations at the Central facility for electron microscopy (GFE), Aachen, another specimen was nickel plated and embedded in a conductive phenol resin (ATM GmbH, Mammelzen, Germany). The cross-section was ground with SiC paper and then polished with a diamond suspension of 3 µm, 1 µm and 0.5 µm. The final polishing was performed with a colloidal 0.05 µm SiO_2 suspension.

Secondary electron (SE) and backscatter (BSE) images, and electron backscatter diffraction (EBSD) measurements, were acquired using a JSM7000F scanning electron microscope (JEOL Tokio, Japan) equipped with a Hikari EBSD camera (Ametek EDAX, Weiterstadt, Germany). The data collection and analysis were performed using the OIM Data Collection and OIM Analysis Software from EDAX-TSL. The usual step size for EBSD measurements is either 50 nm or 100 nm, depending on the grain size and measurement area. The acceleration voltage for EBSD measurements was 15 keV.

2.3.3. X-ray-Diffraction

X-ray diffraction techniques offered insight into the stress state and crystalline structure of the investigated samples. Using the standard $\sin^2\Psi$ method [43], the residual stress state in two orthogonal directions was analyzed on the surface. Depth profiles of the residual stresses were generated at Leibniz-Institute for Materials Engineering—IWT Bremen by stepwise electrochemical material removal. Additional information was obtained through full-width at half maximum (FWHM) values of the measured {211} diffraction peak (XEL: E = 220 GPa, v = 0.28) by comparison with the initial material state. The FWHM gives information about work hardening and other changes in the microstructure [44]. Broadening of the peak is particularly influenced by decreasing the domain size and increasing microstrains [45]. This was used to analyze the dislocation density in surface phase analyses over three diffraction peaks of α-Fe using Rietveld refinement from TOPAS 4.2, and calculating it using the relationship described by Williamson and Smallman [46]. The instrumental peak broadening was convoluted in the Rietveld evaluation using measurements of NIST LaB_6 standard powder. All measurements of residual stress for the different processes were done using Cr-Kα radiation with a vanadium filter in a common template, as shown in Table 8. The intensity of the radiation was recorded with a line detector.

Table 8. Parameters for the measurement of residual stresses by X-ray diffraction.

Parameter Abr. [unit]	Primary Beam Diameter d_b [mm]	Lattice Plane	Tube Voltage U [kV]	Tube Current I [mA]	Ψ Angles 11 between	Step	Range in 2θ
value	2	α{211}	33	40	−45° to +45°	0.1	147 to 163°

3. Results

3.1. Comparison of Hardness Measurement Investigation Results

The results of the Martens hardness measurement are displayed in Figure 5. For an overview of the depth profiles, the results are sorted into pairs. The grey lines in the figures provide the hardness of the initial ferritic-pearlitic microstructures. The solid horizontal line represents the mean value of the hardness of the initial microstructure, whereas the dashed lines represent the standard deviation of the mean value of the hardness.

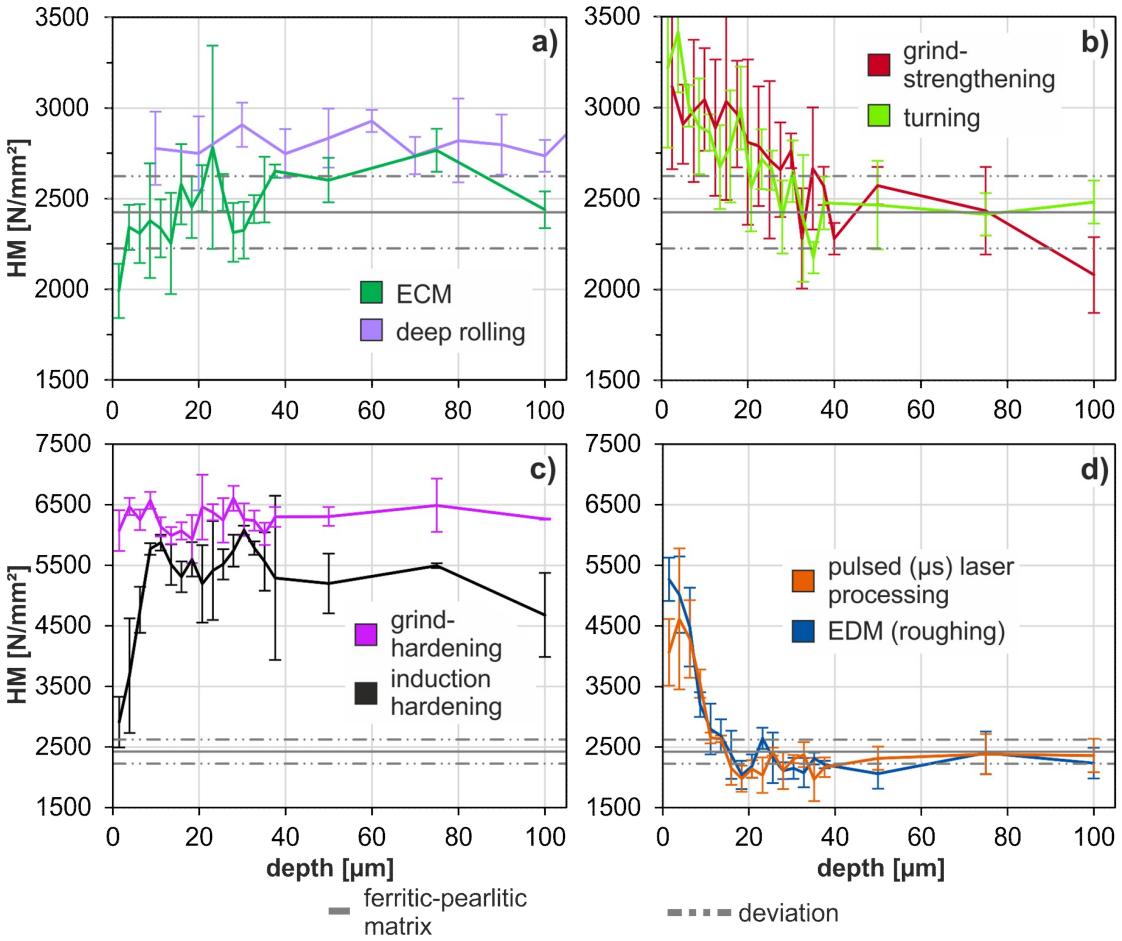

Figure 5. Martens hardness depth profiles of (**a**) ECM and deep rolled surface, (**b**) grind-strengthened and turned surface, (**c**) grind-hardened and induction hardened surface, and (**d**) pulse laser processed and EDM (roughened) surface.

Figure 5a,b have the same hardness scales, allowing us to compare the hardness profiles of deep rolling, ECM (Figure 5a) and grind-strengthening, and turning (Figure 5b). The Martens hardness depth profile of the deep rolled specimen showed the smallest deviation; see Figure 5a (marked in light purple). The measured values were slightly above the hardness of the initial microstructure in the relevant section. Even at a depth of 400 µm, which is not shown in Figure 5a, the hardness was still slightly above that of the initial material. At further depths, the hardness decreased again to the level of the FP material. ECM exerts a chemical impact (see Figure 5a, marked in green). The depth profile of the ECM processed specimen shows that the hardness remained unaffected by the process. Most measured hardness values were in the range of the hardness measured in the initial microstructure. The hardness near the surface area seemed to be slightly reduced, with values near the lower deviation range of the hardness of the initial microstructure.

With the applied process parameters, the grind-strengthening and turning process resulted in similar hardness profiles. In the case of the grind-strengthening process (see Figure 5b, marked in red), a small increase in hardness from the surface up to a depth of 40 µm was observed. From a depth of 40 µm on, the hardness values fluctuated in the range of the hardness of the initial microstructure. The results of the hardness measurements of the turned specimen (see Figure 5b, marked in light green) show an increase in the Martens hardness in the near surface area. From the surface area, the hardness decreased again until it reached the value of the initial microstructure at a depth of about 40 µm.

A comparison of grind-hardening and induction hardening is displayed in Figure 5c. The former FP-matrix was hardened. The grinding process (see Figure 5c, marked in violet) produced a relatively

homogeneous hardness profile. The hardness depth profile, resulting from induction hardening, was less homogeneous. Near the surface, the hardness was not much higher than that of the initial microstructure. At a depth of about 10 µm, the hardness reached the highest level and remained high at further depths.

The results of pulsed (µs) laser processing and the EDM (roughing) process are compared in Figure 5d. For a better comparison, the scale of Figure 5d is the same as that of Figure 5c. The Martens hardness depth profile of the pulsed (µs) laser process (see Figure 5d marked orange) shows a distinct increase in hardness near the surface up to a depth of 10 µm. At a depth of between 15 and 35 µm, the hardness decreased slightly to values below the hardness of the initial microstructure. From a depth of about 40 µm, the hardness increased to the level of the initial microstructure. The Martens hardness depth profile of the EDM (roughing) processed specimen was similar to the pulsed (µs) laser processed specimen hardness profile (see Figure 5d marked blue). The Martens hardness near the surface increased to more than 5000 N/mm^2, but decreased to the values of the initial microstructure at a depth of about 15 µm, and further decreased below those values between 15 and 35 µm. At depths of up to 100 µm, the Martens hardness was again in the range of the initial microstructure.

3.2. Comparison of Electron Microscope Results

In this section, selected SE-micrographs are shown. Figure 6 gives an overview of the microstructures of various cross sections after the different machining processes. The typical initial ferritic-pearlitic microstructure can be detected below the machined surface area in the micrographs f–h. It consists of ferrite grains which appear grey in the micrographs, and pearlite grains that consist of a mixture of ferrite and cementite lamellae. The cementite lamellae appear as bright white lines in the micrographs.

Deep rolling, with the parameters used in this study, did not have any influence on the microstructure visible at this magnification (Figure 6a). The actual microstructural changes that occurred are discussed later in Figure 7a. Grind-strengthening has mainly a mechanical impact on the workpiece. Due to shear deformation, the ferrite-pearlite grains at the surface were heavily deformed. The deformation reduced gradually with depth, and could be detected up to a depth of 5–7 µm. The pearlite lamellae were deformed in grinding direction, to the left side in this micrograph. Beneath the deformed surface layer, the initial ferritic-pearlitic microstructure is visible (Figure 6b).

Turning, a process with a thermo-mechanical impact, is represented in Figure 6c. The figure is divided into a left and a right micrograph. Both show that the cementite lamellae were deformed in the turning direction, to the right side of the micrographs. The left part of the figure shows a very even surface with a near surface layer of heavily deformed cementite lamellae. On the right side, an uneven surface can be detected, where the material was ripped out during the turning process.

For grind and induction hardening, the generated surface layer was too thick to be displayed completely; see Figure 6d,e. Only remnants of the cementite lamellae in the structure of the martensite could be detected. This was caused by the incomplete homogenization of the carbon content in the former pearlitic structure due to the short austenitization duration. As shown in Figure 6d, the remnants of the ferritic-pearlitic microstructure visible in the grind hardened specimen were less pronounced.

A strong thermal influence on the microstructure near the surface can also be seen in Figure 6f, i.e., pulsed (µs) laser processing and g electro discharge machining (roughing). The microstructural changes were caused by temperatures which were far above the austenitization temperature. Pulsed (µs) laser processing and electro discharge machining (roughing) have a short-time temperature impact, limiting the microstructural changes to a small surface region. However, due to the high temperatures that occur, both processes cause major changes in the microstructures of the near surface area.

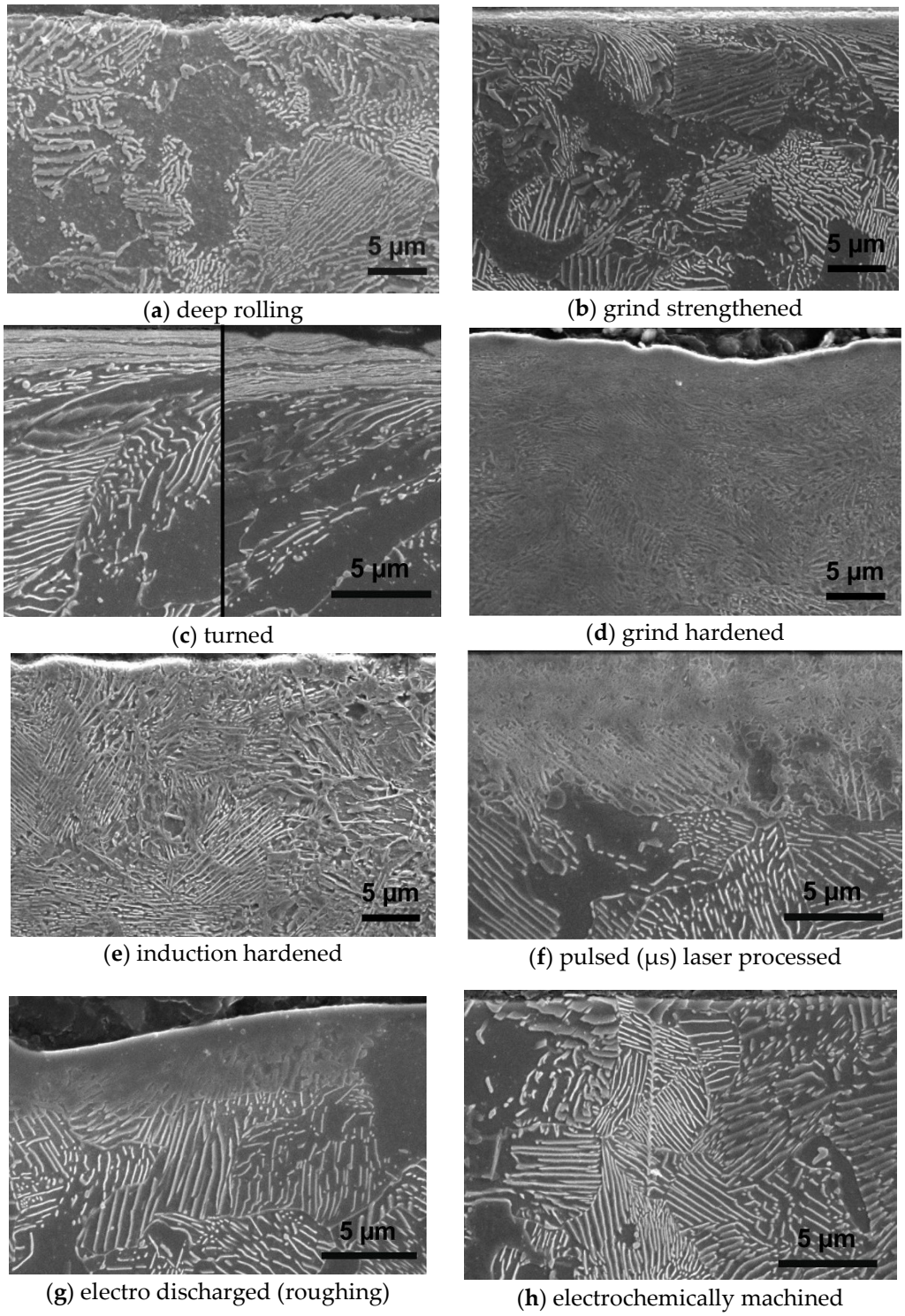

Figure 6. SE-micrographs of (**a**) deep rolled surface, (**b**) grinded strengthened surface, (**c**) turned surface, (**d**) grind hardened surface, (**e**) induction hardened surface (**f**) pulsed (µs) laser processed surface, (**g**) electro discharged (roughing) machined surface and (**h**) electrochemically machined surface.

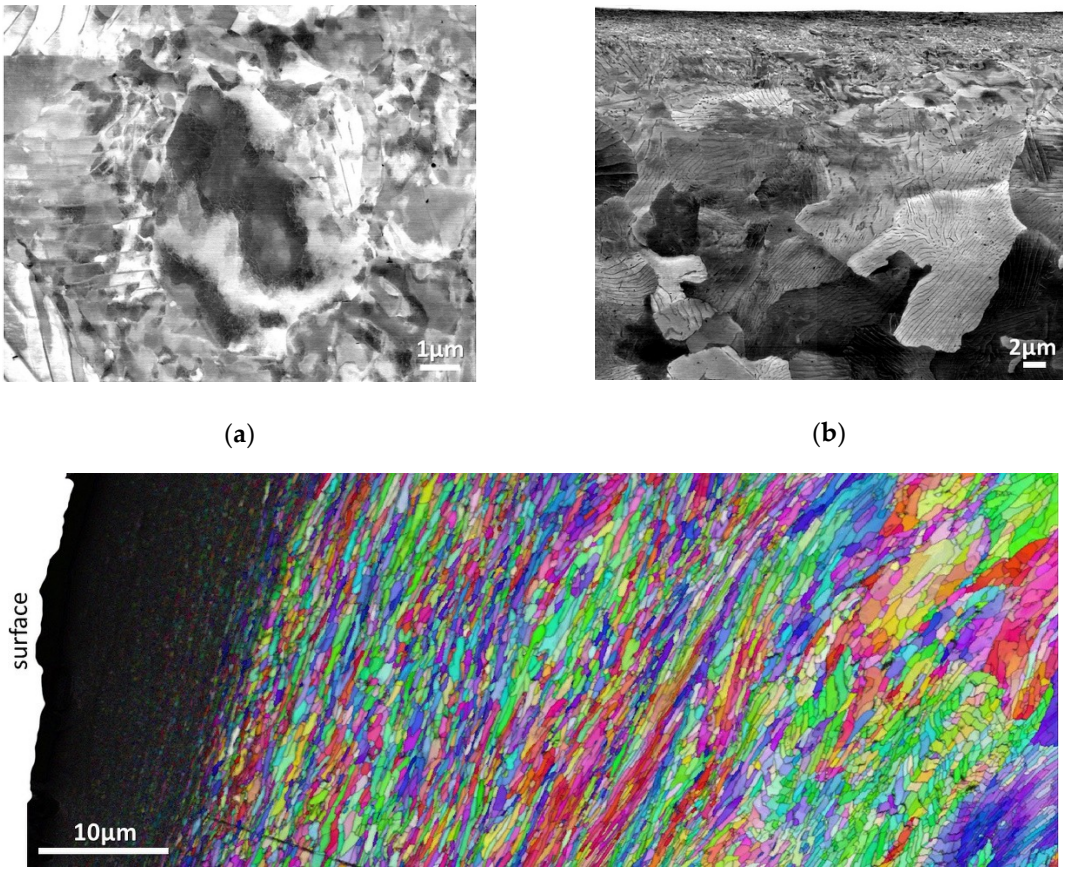

(**a**) (**b**)

(**c**)

Figure 7. (**a**) BSE image of deep rolled cross section, (**b**) BSE image of grind strengthened cross section, (**c**) EBSD Image Quality Map with an overlaid Inverse Pole Figure Map of turned cross section.

The pulsed (µs) laser processed specimen showed a microstructure with a visually changed surface layer of about 10 µm thickness; see Figure 6f. The surface microstructure was inhomogeneous, and remnants of the cementite lamellae could still be found. The carbon content of the cementite was only partially distributed, since the high temperature impact on the workpiece was very short. Originally ferritic areas, for this same reason, remain ferritic.

The EDM cross section shows a homogeneous dark zone at the surface of about 4 µm thickness, and a zone of about 6 µm thickness below, where the original structure of the cementite lamellae of the pearlite grains is still visible in the martensite, due to incomplete carbon dissolution (see Figure 6g). It is known that surfaces modified by EDM usually consist of a recast layer (RL) of resolidified melt and a heat affected zone (HAZ), which is marked by phase transformation. The homogeneous dark zone at the surface may be related to the RL. The layers are described more detail in the description of Figure 8c. The cross section taken from the electrochemically machined surface shows an unaffected initial microstructure (see Figure 6h). On the surface, the ferritic matrix was etched more easily than the cementite lamellae, leading to an almost smooth surface with lamellae sticking out.

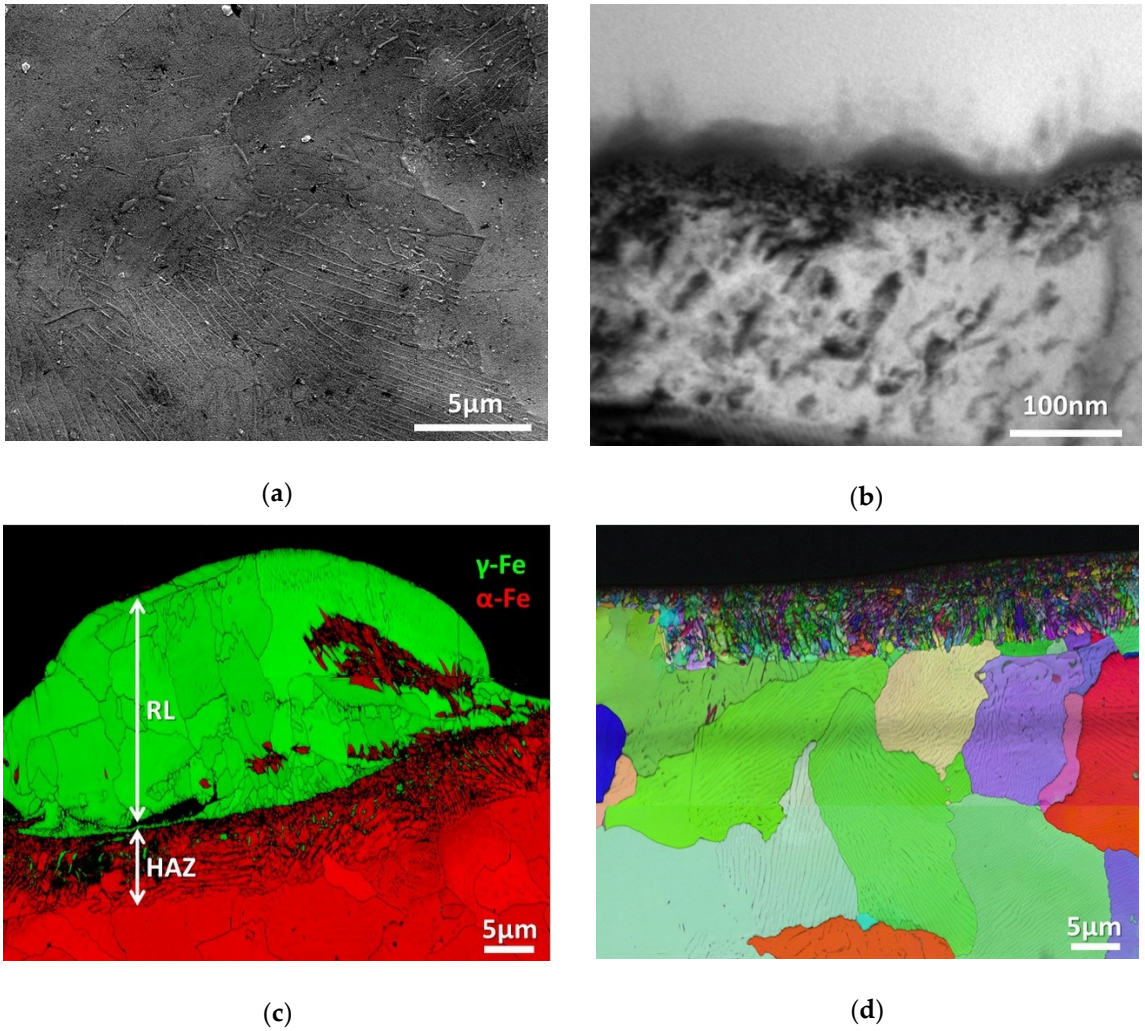

Figure 8. (**a**) SE image of surface of ECM sample, (**b**) BF image of FIB lamella cut from ECM surface, (**c**) EBSD Image Quality Map with overlaid Phase Map of cross section of EDM (roughing) sample, (**d**) EBSD Image Quality Map with overlaid Inverse Pole Figure Map of pulsed (µs) laser processed cross section.

In Figures 7 and 8, examples of further electron microscope investigation of surface zones for different processes are shown. In mechanical processes like deep rolling (Figure 7a) and grind-strengthening (Figure 7b), dislocations are generated, forming dislocation networks. These networks can build subgrain boundaries and either form low angle grains by dynamic recovery (deep rolling (Figure 7a) or nanocrystalline grains by continuous dynamic recrystallization (grind-strengthening (near the surface in Figure 7b). The BSE images distinctly show small variations in grain orientation, as expected for dislocations and other crystal defects. For certain orientations, the dislocation networks can be seen in the BSE images (e.g., in the dark area in the middle of Figure 7a). EBSD measurements allow the quantitative determination of grain sizes, grain orientation and the texture of the deformed surface zone. An inverse pole figure map is shown in Figure 7c for the cross section of the turned surface. Small grains with high angle grain boundaries were formed. Close to the surface, the grains were too small to be detected with EBSD, so TKD (Transmission Kikuchi Diffraction) or TEM methods were necessary for the investigation. During turning, high temperatures can be reached; however, the occurrence of phase transformation was excluded by EBSD and TEM investigations.

ECM is known to have a very small affected surface zone, i.e., only a few tens of nm. An SE image of the surface is shown in Figure 8a. The surface was smooth and shiny. Cementite lamellae were

clearly visible, but there was no pronounced etching of the ferrite phase compared to the cementite phase, as in the other investigations. A bright field (BF) image of a FIB lamella cut from the surface is shown in Figure 8b. A very thin reaction layer of about 50 nm is visible. The reaction layer consisted of oxygen, confirming the formation of oxide layers during the ECM process.

EDM (roughing) (Figure 8c) and pulsed (µs) laser processing (Figure 8d) are processes with mainly thermal impact, where the surface zone is melted by spark erosion and laser radiation, respectively, and resolidified on the surface as a so-called recast layer (RL). Below the RL is the heat affected zone (HAZ), which is marked by phase transformation and the formation of nanocrystalline martensite and retained austenite. Due to the high temperatures involved, cementite lamellae are dissolved. Since the carbon cannot distribute itself homogenously by diffusion, the mostly martensitic microstructure contains retained austenite. Furthermore, the short high temperature heat treatment can only cause a phase transformation of pearlite grains, because the locally enhanced carbon concentration (ferrite ~0.02% C, pearlite ~0.8%) lowers the austenitization temperature and the critical quenching velocity [47]. The dielectric fluid (EDM) is pyrolyzed by the high temperatures, resulting in a carburized RL. High carbon contents change the transformation behavior. The RL therefore consists mostly of austenite and rarely localized Fe_3C inclusions (not visible in this image).

3.3. Evaluation of X-ray Diffraction Measurements

The processes observed in this study induce mechanical, thermal and chemical loads on the material state with different affected depths. A comparison of processes can be made by classifying the observed changes according to their microstructure and residual stress states. For mechanical impact, the deep rolling process is able to exert a high loading strain field deep into the material with local yielding. Plastic deformation can reach hundreds of µm into the material, and material flow is maximal at the surface. However, the peak of compressive residual stresses is generally generated below the surface [45]. This is reflected in Figure 9, where the maximum compressive residual stress with a plateau in the range of the yield strength of the material at −350 MPa from 150 to 400 µm depth can be observed. The compressive residual stresses reached depths of more than 1 mm, as well as the plastically deformed layer, as indicated by an increased FWHM over the entire zone (Figure 9).

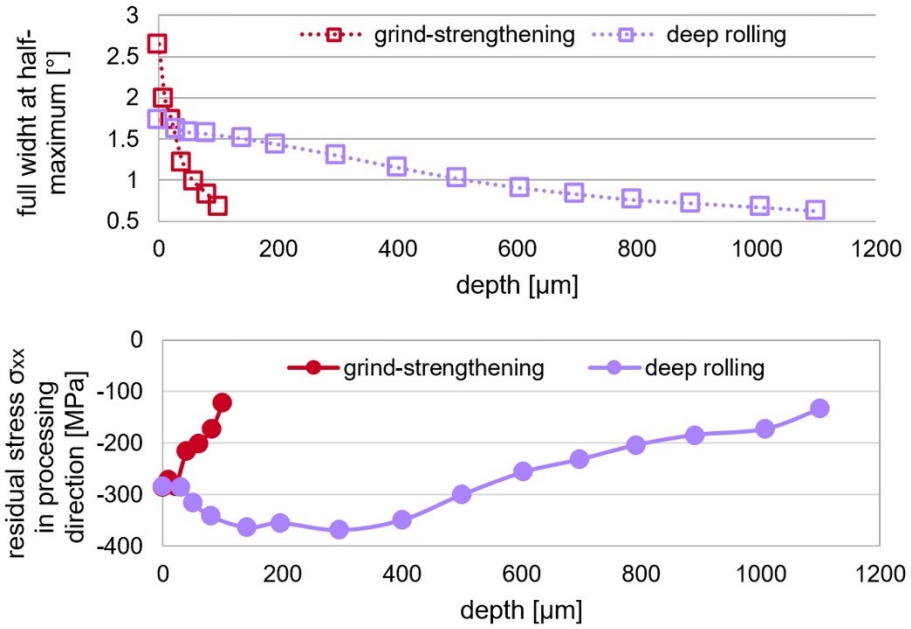

Figure 9. Residual stress and FWHM depth profiles for two processes with main mechanical impact: deep rolling and grind-strengthening.

The grind strengthened state, which is also mainly driven by mechanical impact, exhibits an affected depth which is much lower than after deep rolling. In this case, the internal load condition is generated by stochastic contact of thousands of abrasive grains with a noticeably smaller contact area compared to the deep rolling tool, which strongly limits the depth of the loading strain fields in the material. The highest residual stresses were found directly at the surface, which rapidly decreased in the first 100 µm. In the FWHM distribution, the top surface layers exhibited maximal plastic deformation, i.e., higher than that in the deep rolled condition but with a lower affected depth, as shown in Figure 9.

Deep rolling and grind-strengthening, as processes with mainly mechanical impact, and hard turning, as a thermo-mechanical process, show direction-dependent stress states, partly with additional out-of-plane shear stress components which are also direction dependent, as shown in Figure 10. For comparison, the stress components along the longitudinal direction (processing direction 0°) are written as σ_{xx}, while those in the transversal direction (perpendicular to the process feed direction) are called σ_{yy}. Shear stresses are accordingly referred to as τ_{xz} and τ_{yz}. The results show that, in particular, the deep rolling and the hard turning processes showed strong asymmetrical stresses, while in grind-strengthening, the differences between the normal stress components are small. In contrast, the hard turning process induced high levels of tensile stress due to its thermal impact, while the mechanically driven processes exhibited high levels of compressive stress. Beside the different affected depths in the three processes, the shear stress components were also different. The grind-strengthening and hard turning processes induced, in particular, pronounced shear stresses in the feed direction due to the strong shear deformation of the material in this direction.

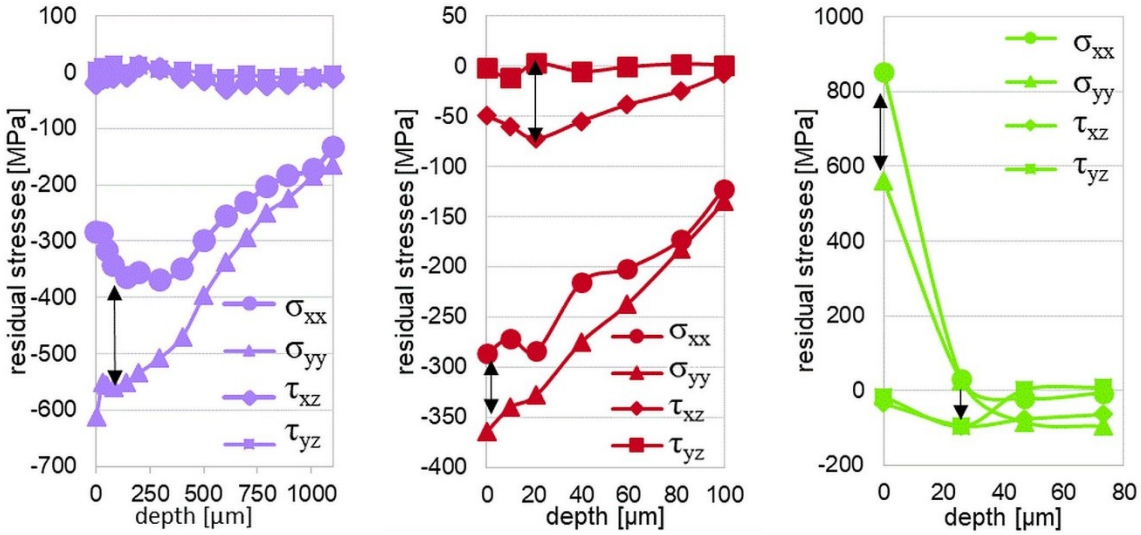

Figure 10. Comparison of residual stresses for three manufacturing processes (deep rolling (**a**), grind-strengthening (**b**) and hard turning (**c**)).

In processes with mainly thermal influence, thermal energy input may lead to short duration austenitization of the outer surface and the creation of a martensitic layer during the subsequent rapid cooling. On the other hand, if the austenitization temperature is not reached, thermally activated effects will take place, in particular, recovery and recrystallization, but also local yielding, leading to residual stress generation. The EDM and pulsed (µs) laser processes (PLP) have very short durations. Even though the processes work differently, the thermal input clearly produced the most residual stresses in both cases. As a result, the statistically distributed electrical discharges of the EDM process led to a direction-independent tensile stress state at a depth of up to 80 µm, while the surface processed

with µs laser pulses exhibited a nonsymmetrical tensile residual stress state with a lower affected depth of 40 µm, as seen in Figure 11. This was caused by the fact that, depending on the laser processing pattern, a specific thermal gradient, as well as differences in the surface phase material state, were exhibited, which produced a difference between the principal residual stress directions.

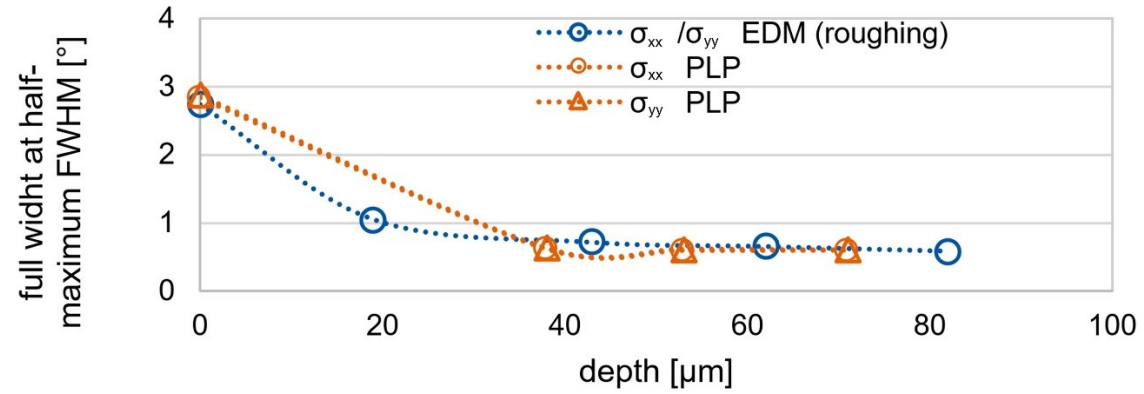

(**a**)

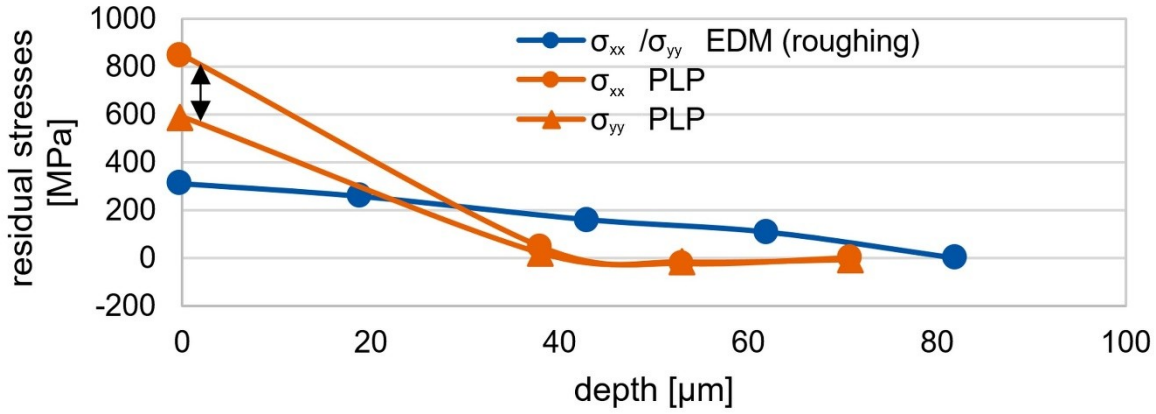

(**b**)

Figure 11. Comparison of the residual stress (**a**) and FWHM depth profiles (**b**) of EDM (roughing) and pulsed (µs) laser processed surfaces (PLP).

When the thermal input was increased considerably, the depth of hardened layers could be extended, as, for example, in the induction hardening process (Figure 12). In contrast to the surface energy input of the pulsed (µs) laser process, the volume heating in this case led to phase changes in the range of hundreds of µm, which, in turn, led to compressive residual stresses in the surface region up to several millimeters and compensating tensile stresses below the hardened layer. The grind-hardening process can be considered as comparable concerning the achievable residual stress state.

The processes, their corresponding mechanisms and the detectable modifications are listed in Table 9.

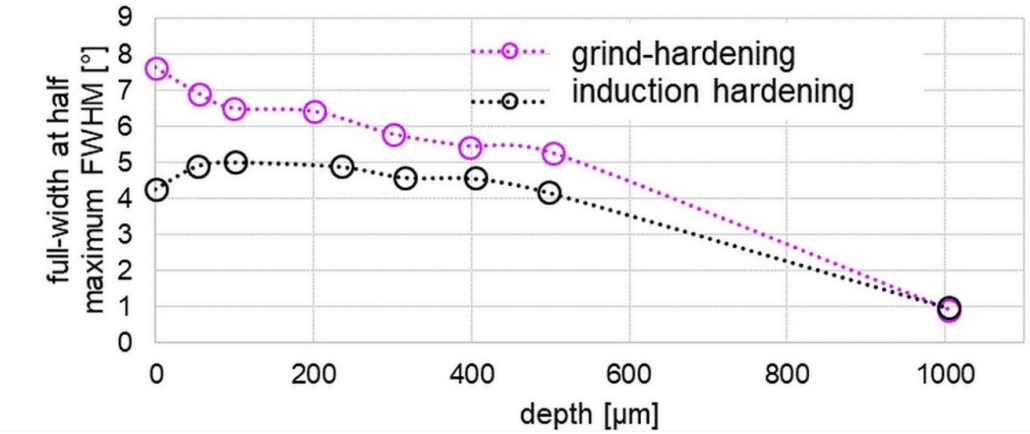

(**a**)

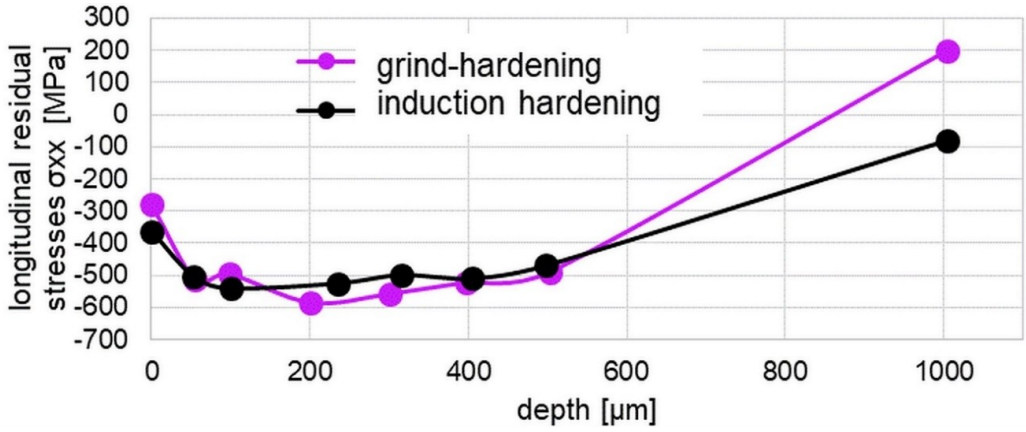

(**b**)

Figure 12. Longitudinal residual stress (**a**) and FWHM depth profiles (**b**) for thermally dominated processes: induction hardening and grind-hardening.

Table 9. Comparison of mechanisms and electron microscopically measurable modifications for different manufacturing processes.

Process	Main Impact	Mechanisms	Measured Modifications
deep rolling	mechanical	dislocation formation/accumulation/ rearrangement, dynamic recovery, work hardening	compressive residual stresses, dislocation density, dislocation arrangements, subgrain boundaries, misorientation
grind-strengthening	mechanical	dislocation formation/accumulation/ rearrangement, continuous dynamic recrystallization, work hardening	compressive residual stresses, shear stresses, dislocation density, misorientation, grain sizes, texture
hard turning	thermo-mechanical	continuous dynamic recrystallization, work hardening, annealing	residual stresses, shear stresses, dislocation density, misorientation, grain sizes, texture

Table 9. *Cont.*

Process	Main Impact	Mechanisms	Measured Modifications
grind-hardening	thermo-mechanical	continuous dynamic recrystallization, phase transformation, diffusion of carbon, annealing	residual stresses, grain sizes, carbon diffusion, phase contents
induction hardening	thermal	diffusion, phase transformation	residual stresses, grain sizes, carbon diffusion, phase contents
pulsed (µs) laser processing	thermal	melting/solidification, diffusion, phase transformation	residual stresses, dislocation density, grain sizes, carbon diffusion, phase contents, dendrite arm distances
EDM (roughing)	thermo-chemical	melting/solidification, phase transformation, diffusion	residual stresses, dislocation density, grain sizes, carbon diffusion, phase contents, dendrite arm distances
ECM	chemical	local dissolution of phases, chemical reactions	phase concentration, oxides and nitrates in surface zone

4. Discussion

The results of the combined analysis techniques give a good outline of the characteristics and depth of the material modifications and the underlying mechanisms. In the case of deep rolling, there was good agreement between the hardness, the FWHM and the residual stresses. The depth profiles of the different analysis techniques showed the modifications at comparable depths. The hardness measurement was not the best method for analyzing modifications caused by work hardening effects, since the characteristic mechanisms are the formation of dislocation networks and dynamic recovery. Deep rolling with only a mechanical impact on the material had, due to the Hertzian contact condition, the highest mechanical impact underneath the surface. It also had the greatest depth effect caused by mechanical impact.

The hardness increase observed after hard turning and grind-strengthening (Figure 5c) could be interpreted thanks to the results of electron microscopy, as shown in Figure 7b,c. Both processes showed an enhancement in the dislocation density and grain refinement in the surface layer. The grain refinement occurred due to continuous dynamic recrystallization, which was triggered by the (thermo)-mechanical process impact. There is a correlation between hardness and grain size. Finer grains led to an increased hardness (Hall-Petch correlation). Though grind-strengthening is a process with a more mechanical impact, and turning is a process with a thermo-mechanical effect, both led to grain refinement and similar hardness depth profiles. At further depths, plastic deformation predominated as the significant influence.

Due to the different impacts (thermo-mechanical for turning and mechanical for grind-strengthening), the resulting residual stress states were different. Intense plastic deformation of the surface layer due to the mechanical impact caused local positive strain, which left, after the stress had subsided, compressive residual stresses. High local thermal impact caused, due to local hindrance of thermal expansion, tensile residual stresses in the surface.

Consideration of the processes with a high thermal impact showed that extent, duration and affected depth were the main influencing factors for the resulting modifications. The EDM and PLP processes led to maximal hardness at or near the surface. The EDM sample exhibited a recast layer consisting of retained, carbon enriched austenite and nanostructured martensite, as well as sparsely distributed carbide grains which resulted in a maximum hardness of ~5300 N/mm^2. In the heat affected

zone, the hardness decreased towards the bulk material, since the proportion of phase transformation to martensite was reduced. The results of the residual stress measurement of the EDM (roughing) and pulsed (µs) laser processes, however, showed high tensile residual stresses at the surface due to the very high applied temperatures, which resulted not only in phase transformations, but partially also in a recast layer. The processes with a more controlled energy input over a longer duration achieved a greater hardening depth and compressive stresses at the surface. In the case of induction hardening, a volume heat source acts on greater depths of the material. The phase transformation in the range of several hundreds of µm causes, due to the associated increase in volume, the generation of compressive residual stresses in the surface area up to several millimeters depths. In this way, the grind-hardening process, where energy input takes place exclusively at the surface, leads to the formation of a deep hardened layer with comparable compressive residual stresses as after induction hardening. The evolution of residual stresses always involves interactions among local thermal expansion, phase transformation and the temperature-dependent yield strength. If the local yield strength is exceeded, local plastic deformation occurs. Local positive plastic deformation results in local compressive residual stresses, while local compressive deformation results in local tensile residual stresses. However, the component must remain in balance with itself.

The results of an analysis of the ECM process with a chemical impact reveal that, also for these processes, surface modification occurred. In this case, a 50 nm thick oxidation zone can be recognized.

In Figure 13 the different microstructure modifications and their penetration depths for the different processes are presented. As can be seen, similar modifications were achieved by different mechanisms using different processes. For instance, nanocrystalline grains in the first µm of the surface zone were generated by massive shear deformation (grinding and turning processes) or by rapid phase transformations (EDM and laser polishing). Additionally, the same modifications can be generated at a wide variety of penetration depths, depending on the process. A phase transformed microstructure could be generated by grind-hardening, EDM and laser polishing but the penetration depth of the phase transformed surface zone varied, depending on the process, from between a few µm and several hundreds of µm.

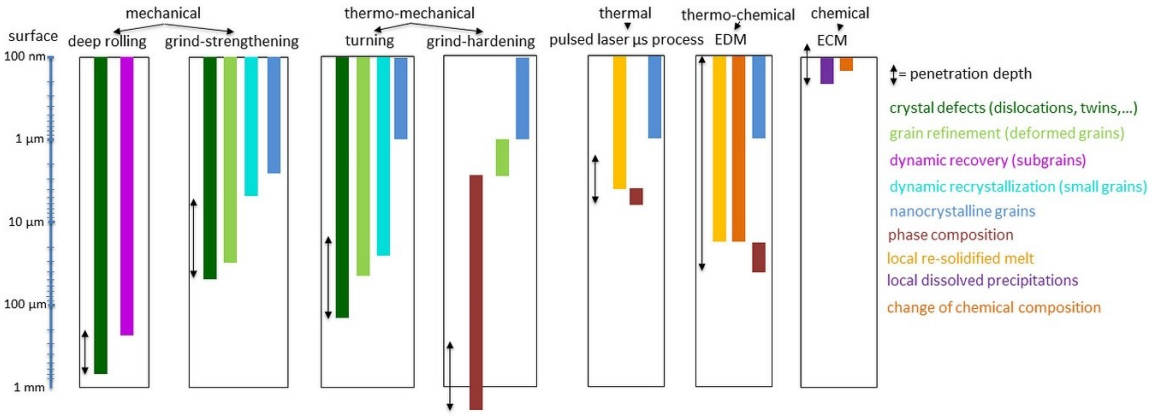

Figure 13. Comparison of microstructure modifications and their modification depth caused by different machining operations (based on [48]).

As stated, in most cases, material modifications are confined to within a certain surface layer, where chemical, microstructural changes and residual stress states are induced.

Figures 14 and 15 present a final comparison between the different processes regarding the surface residual stresses and the determined dislocation densities, together with the respective affected depths of the measurable residual stress that were found before their transition into compensation stresses with a grouping of the modification mechanism. It can be observed by comparing the modifications regarding the amount and type of residual stresses (tensile/compressive) that these depend on mainly mechanical, thermal or chemical mechanisms, as presented in the sections for each

process. However, the depths at which the materials were affected, as written inside the bars for each process, varied greatly depending on the processing parameters, even if the mechanisms remained the same. The dislocation density was increased for all processes by at least one order of magnitude due to local plastic deformation and/or the generation of a martensitic layer. However, the state after ECM processing was comparable to the initial state.

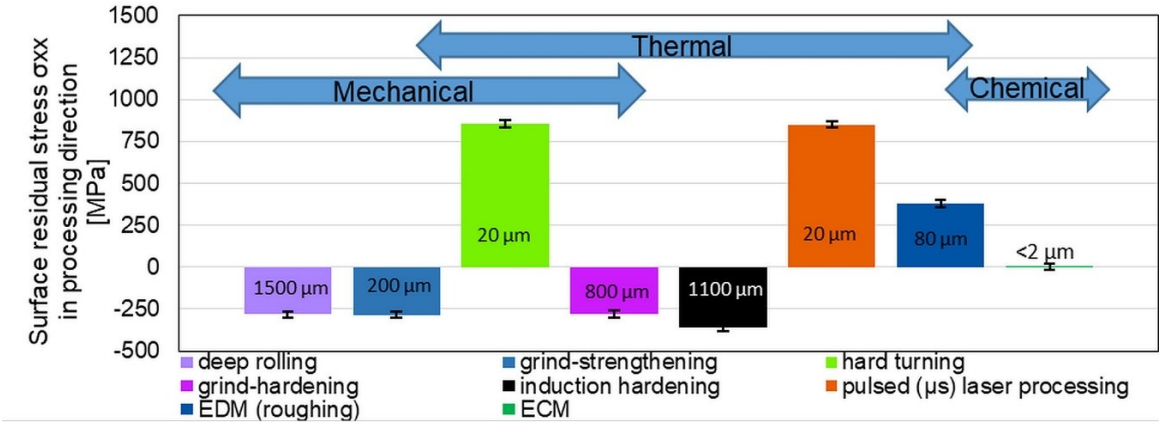

Figure 14. Comparison of the investigated processes regarding the residual stresses at the surface and the affected depth.

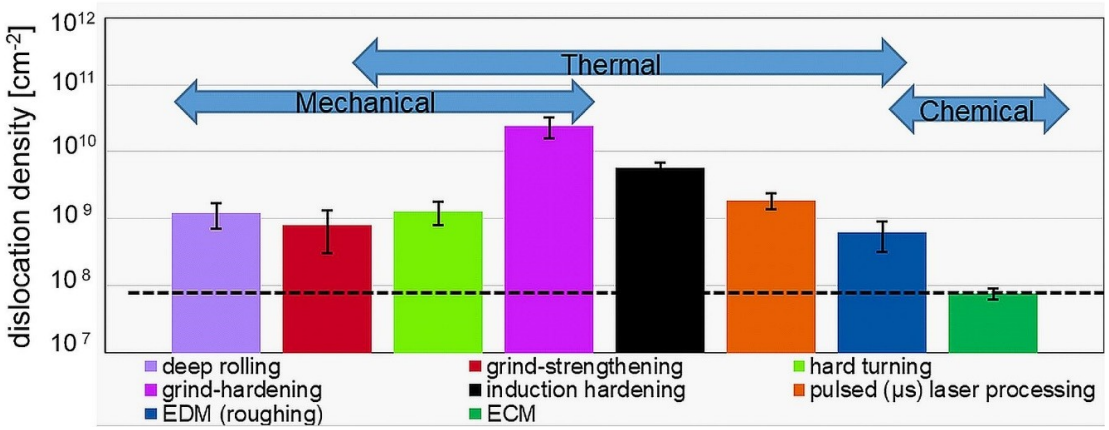

Figure 15. Comparison of the investigated processes regarding the dislocation density at the surface and the affected depth.

For chemically induced process mechanisms, it is shown that the removal of material without thermal or mechanical influence led to no measurable changes in either the residual stress state or the dislocation density within the investigated volume when measured with standard XRD methods. Modifications were confined to a few tens or hundreds of nanometers. Additionally, no detectable additional crystalline phases, aside from the austenite formed with additional carbon, were found on the surface of the EDM specimens with the standard XRD method setup for residual stress and phase analyses. Other thermally dominated processes, including pulsed (µs) laser processing, induction hardening, grind-hardening and hard turning processes, also allowed additional chemical mechanisms to occur, due to the high surface temperatures and suitable surrounding media. If present, these effects were limited to very thin surface layers.

5. Conclusions

The results of this study provide a comprehensive summary of the material modifications found in several present manufacturing processes, as analyzed using a diverse array of methods. For the

first time, an overview concerning the material modifications that may be expected for a given set of processes due to different mechanisms is given. These results might even allow one to speculate about which kind of modifications are to be expected for other processes with similar internal loads.

For mechanical dominated processes like deep rolling and grind-strengthening, dislocation formation and the rearrangement and formation of dislocation cells resulted in work hardening of the material, dynamic recovery (for deep rolling) and continuous dynamic recrystallization effects (for grind-strengthening). Due to the massive shear deformation during grind-strengthening, nanocrystalline grains formed at the surface. The plastic deformation of both processes resulted in compressive residual stresses, but for grind-strengthening only, a significant increase in hardness was observed. For thermo-mechanical processes like turning and grind-hardening, the amount of generated frictional heat heavily influenced the mechanisms of modification. For turning, almost the same microstructural modifications could be found as those for grind-strengthening, since continuous dynamic recrystallization occurred, causing the formation of nanocrystalline grains and an increase in hardness. However, due to the high thermal influence, the residual stresses were tensile in nature. For grind-hardening and induction hardening, the austenitization temperature was reached over a broader surface region, which resulted in massive phase transformation with an increase in hardness and compressive residual stresses.

For the thermo-(chemical) processes like EDM and pulsed (µs) laser processing, a phase transformed and, depending on the parameters, redeposited resolidified melt could be identified on the surface zone. Due to the local introduction of high temperatures, tensile residual stresses could be measured at the surface. The hardness increase at the surface of the EDM samples may largely be attributed to the formation of nanocrystalline martensite grains.

For the chemical process ECM, only a very thin reaction layer, i.e., of ~50 nm thickness, was found. No change in residual stresses compared to the initial material were found, as neither mechanical nor thermal effects influenced the surface. Since the lack of change in the surface condition was paired with the removal rate of up to 1–5 cm^3/min, ECM showed its advantages, especially in combination with other processes with a positive depth effect, but also negative effects, like oxidation or tensile residual stresses on the outer surface.

The different characterization methods showed that hardness measurements and light microscopy, though they might be the fastest and least expensive characterization methods, do not give enough detailed information about the occurring mechanisms and modifications to allow comparisons to be made among different processes. Electron microscopic characterization methods revealed the most information about the microstructures and the underlying mechanisms, but are quite time-consuming, especially for processes with huge penetration depths like deep rolling, grind-hardening and induction hardening. XRD measurements give information not only regarding the type of residual stress that has occurred, but also about the penetration depth. A further evaluation of the observed measurement peaks will reveal information about the dislocation density and the crystal size. With electron microscopy, locally occurring effects like grain refinement or dislocation accumulation could be accurately determined, whereas XRD provided more global description of sample regions.

Author Contributions: Conceptualization, B.C. and R.S.; investigation, F.B., S.E., L.E., S.H., M.H., E.K., H.M., S.S. and R.S.; project administration, B.C., J.E. and A.K.; validation, F.B., S.E., L.E., J.E., S.H., M.H., E.K., H.M., M.M., B.R., S.S. and R.S.; writing—original draft, F.B., S.E., L.E., M.H., E.K., H.M., M.M, B.R., S.S. and R.S.; writing—review & editing, B.C., J.E. and A.K. All authors have read and agreed to the published version of the manuscript.

Funding: This research was funded by German Research Foundation (DFG) with the project number 223500200–TRR 136.

Acknowledgments: The authors thank the German Research Foundation (DFG) for funding the transregional Collaborative Research Center "Process Signatures" with the project number 223500200–TRR 136 (Aachen, Bremen, Oklahoma).

Conflicts of Interest: The authors declare no conflict of interest.

References

1. Jawahir, I.S.; Brinksmeier, E.; M'Saoubi, R.; Aspinwall, D.K.; Outeiro, J.C.; Meyer, D.; Umbrello, D.; Jayal, A.D. Surface integrity in material removal processes: Recent advances. *CIRP Annals Manuf. Technol.* **2011**, *60*, 603–626. [CrossRef]
2. Field, M.; Koster, W. Optimizing grinding parameters to combine high productivity with high surface integrity. *CIRP Ann Manuf. Technol.* **1978**, *27*, 523–526.
3. Gerstenmeyer, M.; Hartmann, J.; Zanger, F.; Schulze, V. Adjustment of Lifetime-Increasing Surface Layer States by Complematary Machining. *HTM J. Heat Treat. Mater.* **2019**, *74*, 181–190. [CrossRef]
4. Brinksmeier, E.; Meyer, D.; Heinzel, C.; Lübben, T.; Sölter, J.; Langenhorst, L.; Frerichs, F.; Kämmler, J.; Kohls, E.; Kuschel, S. Process Signatures—The Missing Link to Predict Surface Integrity in Machining. *Proc. CIRP* **2018**, *71*, 3–10. [CrossRef]
5. Speidel, A.; Mitchell-Smith, J.; Bisterov, I.; Clare, A.T. The importance of microstructure in electrochemical jet processing. *J. Mater. Proc. Technol.* **2018**, *262*, 459–470. [CrossRef]
6. Speidel, A.; Mitchell-Smith, J.; Bisterov, I.; Clare, A.T. The dependence of sur-face finish on material precondition in EC jet machining. *Procedia CIRP* **2018**, *68*, 477–482. [CrossRef]
7. Maradia, U.; Filisetti, E.; Boccadoro, M.; Roten, M.; Dutoit, J.-M.; Hengsberger, S. Increasing the injection moulding productivity through EDM surface modulation. *Proc. CIRP* **2018**, *68*, 58–63. [CrossRef]
8. Berstein, G.; Fuchbauer, B. Festwalzen und Schwingfestigkeit. *Materialwiss. Werkst.* **1982**, *13*, 103–109. [CrossRef]
9. Kocke, F.; Liermann, J. Roller burnishing of hard turned surfaces. *Int. J. Mach. Tools Manuf.* **1998**, *38*, 419–423. [CrossRef]
10. Röttger, K.; Wilcke, G.; Mader, S. Festwalzen—Eine Technologie für effizienten Leichtbau. *Mater. Werkst. Entwickl. Fert. Prüf. Eigenschaften Anwend. Tech. Werkst.* **2005**, *36*, 270–274. [CrossRef]
11. Röttger, K. Walzen Hartgedrehter Oberflächen. Ph.D. Dissertation, RWTH Aachen University, Aachen, Germany, 2003.
12. Lauwers, B.; Klocke, F.; Klink, A.; Tekkaya, A.E.; Neugebauer, R.; McIntosh, D. Hybrid processes in manufacturing. *CIRP Ann. Manuf. Technol.* **2014**, *63*, 561–583. [CrossRef]
13. Klocke, F.; Ehle, L.; Hensgen, L.; Klink, A.; Schwedt, A. Structure and Composition of the White Layer in the Wire-EDM Process. *Proc. CIRP* **2016**, *42*, 673–678. [CrossRef]
14. Ehle, L.; Kämmler, J.; Meyer, D.; Schwedt, A.; Mayer, J. Electron Microscopic Characterization of Mechanically Modified Surface Layers of Deep Rolled Steel. *Proc. CIRP* **2016**, *45*, 367–370. [CrossRef]
15. Heinzel, C.; Borchers, F.; Berger, D.; Ehle, L. Surface and material modifications of tempered steel after precision grinding with electroplated coarse grained diamond wheels. *Proc. CIRP* **2016**, *45*, 191–194. [CrossRef]
16. Malkin, S.; Guo, C. *Grinding Technology: Theory and Application of Machining with Abrasives*; Industrial Press: New York, NY, USA, 2008.
17. Klocke, F. *Manufacturing Processes 2: Grinding, Honing, Lapping*; Springer Verlag: Berlin/Heidelberg, Germany, 2009.
18. Heinzel, C.; Bleil, N. The Use of the Size Effect in Grinding for Work-hardening. *CIRP Ann.* **2007**, *56*, 327–330. [CrossRef]
19. Ehle, L.; Kohls, E.; Richter, S.; Spille, J.; Schwedt, A.; Mayer, J. Grind-hardening: Correlations between surface modifications and applied internal loads. *Proc. CIRP* **2018**, *71*, 341–347. [CrossRef]
20. Buchkremer, S. Irreversible Thermodynamics of Nano-Structural Surface Modifications in Metal Cutting. Ph.D. Dissertation, RWTH Aachen University, Aachen, Germany, 2017.
21. Caruso, S.; Umbrello, D.; Outeiro, J.; Filice, L.; Micari, F. An experimental investigation of residual stresses in hard machining of AISI 52100 steel. *Proc. Eng.* **2011**, *19*, 67–72. [CrossRef]
22. Brunst, W. *Die induktive Wärmebehandlung*; Springer-Verlag: Berlin/Göttingen/Heidelberg, Germany, 1957.
23. Pfeifer, H. *Taschenbuch—Industrielle Wärmetechnik: Grundlagen Berechnungen Verfahren*, 4th ed.; Vulkan-Verlag GmbH: Essen, Germany, 2007.

24. Moreaux, F.; Archambault, P.; Beck, G.; Pourprix, Y. Induktives Randschichthärten von Stahl Ck 45 durch Abschrecken in zerstäubtem Wasser. *HTM Härt. Tech. Mitt.* **1989**, *44*, 129–132.
25. Liedtke, D.; Stiele, H. *Merkblatt 236: Wärmebehandlung von Stahl—Randschichthärten*; Stahl-Informations-Zentrum: Düsseldorf, Germany, 2009.
26. Rudnev, V.; Loveless, D.; Cook, R.; Black, M. *Handbook of Induction Heating, Dekker*; CRC Press: New York, NY, USA, 2003.
27. Poprawe, R. *Laser Application Technology*; Springer: Berlin, Germany, 2011.
28. Tu, J.; Paleocrassas, A.G.; Reeves, N.; Rajule, N. Experimental characterization of a micro-hole drilling process with short micro-second pulses by a CW single-mode fiber laser. *Opt. Lasers Eng.* **2014**, *55*, 275–283. [CrossRef]
29. Olsen, F.O.; Alting, L. Pulsed Laser Materials Processing, ND-YAG versus CO_2 Lasers. *CIRP Ann.* **1995**, *44*, 141–145. [CrossRef]
30. Leitz, K.-H.; Redlingshöfer, B.; Reg, Y.; Otto, A.; Schmidt, M. Metal Ablation with Short and Ultrashort Laser Pulses. *Phys. Proc.* **2011**, *12*, 230–238. [CrossRef]
31. Voisey, K.T.; Kudesia, S.S.; Rodden, W.S.O.; Hand, D.P.; Jones, J.D.C.; Clyne, T.W. Melt ejection during laser drilling of metals. *Mater. Sci. Eng. A* **2003**, *356*, 414–424. [CrossRef]
32. Zhao, T.; Eckert, S.; Vollertsen, F. Recast Zone and Unmelted Zone of the White Layer Induced by Microsecond Pulsed Laser Surface Processing of 42CrMo4 Alloy steel. *Lasers Eng. (Old City Publ.)* **2018**, *41*, 349–358.
33. Kunieda, M.; Lauwers, B.; Rajurkar, K.; Schumacher, B. Advancing EDM through Fundamental Insight into the Process. *CIRP Ann. Manuf. Technol.* **2005**, *54*, 64–87. [CrossRef]
34. Gommeringer, A.; Schmitt-Radloff, U.; Ninz, P.; Kern, F.; Klocke, F.; Schneider, S.; Holsten, M.; Klink, A. EDM-machinable Ceramics with Oxide Matrix. Influence of Particle Size and Volume Fraction of the Electrical Conductive Phase on the Mechanical and Electrical Properties and the EDM Characteristics. *Proc. CIRP* **2018**, *68*, 22–27. [CrossRef]
35. Klocke, F.; Hensgen, L.; Klink, A.; Mayer, J.; Schwedt, A. EBSD-Analysis of Flexure Hinges Surface Integrity Evolution via Wire-EDM Main and Trim Cut Technologies. *Proc. CIRP* **2014**, *13*, 237–242. [CrossRef]
36. Klocke, F.; König, W. *Fertigungsverfahren 3. Abtragen, Generieren, Lasermaterialbearbeitung*; Springer: Berlin, Germany, 2007.
37. Klocke, F.; Schneider, S.; Harst, S.; Welling, D.; Klink, A. Energy-based Approaches for Multi-scale Modelling of Material Loadings during Electric Discharge Machining (EDM). *Proc. CIRP* **2015**, *31*, 191–196. [CrossRef]
38. Murali, M.; Yeo, S.-H. Process Simulation and Residual Stress Estimation of Micro-Electrodischarge Machining Using Finite Element Method. *Jpn. J. Appl. Phys.* **2005**, *44*, 5254–5263. [CrossRef]
39. Bergs, T.; Schneider, S.; Harst, S.; Klink, A. Numerical simulation and validation of material loadings during electrical discharge machining. *Proc. CIRP* **2019**, *82*, 14–19. [CrossRef]
40. Mujumdar, S.; Curreli, D.; Kapoor, S.; Ruzic, D. A Model of Micro Electro-Discharge Machining Plasma Discharge in Deionized Water. *J. Manuf. Sci. Eng.* **2014**, *136*, 031011. [CrossRef]
41. Ehle, L.; Schneider, S.; Schwedt, A.; Richter, S.; Klink, A.; Mayer, J. Electron microscopic characterization of surface zones thermo-chemically modified by electrical discharge machining. *J. Mater. Process. Technol.* **2020**, *280*, 116596. [CrossRef]
42. Klocke, F.; Schneider, S.; Ehle, L.; Meyer, H.; Hensgen, L.; Klink, A. Investigations on Surface Integrity of Heat Treated 42CrMo4 (AISI 4140) Processed by Sinking EDM. *Proc. CIRP* **2016**, *42*, 580–585. [CrossRef]
43. Noyan, I.C.; Cohen, J.B. *Residual Stress: Measurement by Diffraction and Interpretation*; Springer-Verlag: Berlin/Göttingen/Heidelberg, Germany, 2013.
44. Nikitin, I.; Scholtes, B.; Maier, H.-J.; Altenberger, I. High temperature fatigue behavior and residual stress stability of laser-shock peened and deep rolled austenitic steel AISI 304. *Scr. Mater.* **2004**, *50*, 1345–1350. [CrossRef]
45. Meyer, H.; Epp, J.; Zoch, H.-W. Residual stress and dislocation density development in single track deep rolled AISI 4140H steel. *Proc. CIRP* **2018**, *71*, 192–197. [CrossRef]
46. Williamson, G.K.; Smallman, R.E., III. Dislocation densities in some annealed and cold-worked metals from measurements on the X-ray Debye-Scherrer spectrum. *Philos. Mag.* **1956**, *1*, 34–46. [CrossRef]

47. Orlich, J.; Rose, A.; Wiest, P. Zeit-Temperatur-Austenitisierungs-Schaubilder. In *Atlas zur Wärmebehandlung der Stähle, MPI. f*; Eisenforschung/Verlag Stahleisen: Düsseldorf, Germany, 1973.
48. Ehle, L.; Schwedt, A.; Richter, S.; Aretz, A.; Weirich, T.; Mayer, J. Characterization of mechanical, thermal, thermo-mechanical and chemical modified surface zones by different electron microscopic methods. Poster Presentation on 19th International Microscopy Congress, Sydney, Australia, 9–14 September 2018. ID290.

© 2020 by the authors. Licensee MDPI, Basel, Switzerland. This article is an open access article distributed under the terms and conditions of the Creative Commons Attribution (CC BY) license (http://creativecommons.org/licenses/by/4.0/).